Title:

Combination of synthetic chemistry and live-cell imaging identified a rapid cell division inhibitor in tobacco and *Arabidopsis thaliana*

Running Title:

Synthesis of a novel cell division inhibitor

Corresponding Authors:

1. Minako Ueda (Institute of Transformative Bio-Molecules (ITbM), Nagoya University, Furo-cho, Chikusa-ku, Nagoya, Aichi 464-8602, Japan; Tel.: + 81 52 747-6402; Fax.: + 81 52 747-6405; Email: m-ueda@itbm.nagoya-u.ac.jp)

2. Masakazu Nambo (Institute of Transformative Bio-Molecules (ITbM), Nagoya University, Furo-cho, Chikusa-ku, Nagoya, Aichi 464-8602, Japan; Tel.: + 81 52 788-6245; Fax.: + 81 52 747-6866; Email: mnambo@itbm.nagoya-u.ac.jp)

Subject Areas:

(1) growth and development, (11) new methodology

Number of black and white figures, color figures, tables and type and number of supplementary material:

Black and white figures; 0

Color figures; 7

Tables; 0

Supplementary materials: 3 tables, 3 figures, 1 movie, and 1 method

Title and running head:

Combination of synthetic chemistry and live-cell imaging identified a rapid cell division inhibitor in tobacco and *Arabidopsis thaliana*

Synthesis of a novel cell division inhibitor

Authors:

Masakazu Nambo[1,*], Daisuke Kurihara[2,3], Tomomi Yamada[1], Taeko Nishiwaki-Ohkawa[1,4], Naoya Kadofusa[4], Yusuke Kimata[2], Keiko Kuwata[1], Masaaki Umeda[5,6], and Minako Ueda[1,2,*]

Author's Addresses:

[1]Institute of Transformative Bio-Molecules (ITbM), Nagoya University, Furo-cho, Chikusa-ku, Nagoya, Aichi 464-8602, Japan

[2]Division of Biological Science, Graduate School of Science, Nagoya University, Furo-cho, Chikusa-ku, Nagoya, Aichi 464-8602, Japan

[3]JST, ERATO Higashiyama Live-Holonics Project, Nagoya University, Furo-cho, Chikusa-ku, Nagoya, Aichi 464-8602, Japan

[4]Laboratory of Animal Physiology, Department of Applied Molecular Biosciences, Graduate School of Bioagricultural Sciences, Nagoya University, Furo-cho, Chikusa-ku, Nagoya, Aichi 464-8601, Japan

[5]Laboratory of Plant Growth Regulation, Graduate School of Biological Sciences, Nara Institute of Science and Technology (NAIST), Takayama-cho 8916-5, Ikoma, Nara 630-0192, Japan

[6]JST, CREST, Takayama-cho 8916-5, Ikoma, Nara 630-0192, Japan

Abbreviations:

BY-2, Bright Yellow-2; CenH3, centromeric histone H3; CLT, clotrimazole; DAG, days after germination; DMSO, dimethylsulfoxide; Fucci, Fluorescent Ubiqutination-based Cell Cycle Indicator; GFP, green fluorescent protein; GT, GFP-α-tubulin; GTRC, GFP-α-tubulin and RFP-CenH3; M phase, mitotic phase; PI,

propidium iodide; PM, proximal meristem; RFP, red fluorescent protein; S phase, synthesis phase; STLC, *S*-trityl-L-cysteine; YFP, yellow fluorescent protein

Footnotes:

*These authors contributed equally to the article.

Abstract:

Cell proliferation is crucial to the growth of multicellular organisms, and thus the proper control of cell division is important to prevent developmental arrest or overgrowth. Nevertheless, tools for controlling cell proliferation are still poor in plant. To develop novel tools, we focused on a specific compound family, triarylmethanes, whose members show various antiproliferative activities in animals. By combining organic chemistry to create novel and diverse compounds containing the triarylmethyl moiety and biological screens based on live-cell imaging of a fluorescently labeled tobacco BY-2 culture cell line (*Nicotiana tabacum*), we isolated (3-furyl)diphenylmethane as a strong but partially reversible inhibitor of plant cell division. We also found that this agent had efficient antiproliferative activity in developing organs of *Arabidopsis thaliana* without causing secondary defects in cell morphology, and induced rapid cell division arrest independent of the cell cycle stage. Given that (3-furyl)diphenylmethane did not affect the growth of a human cell line (HeLa) and a budding yeast (*Saccharomyces cerevisiae*), it should act specifically on plants. Taking our results together, we propose that the combination of desired chemical synthesis and detailed

biological analysis is an effective tool to create novel drugs, and that (3-furyl)diphenylmethane is a specific antiproliferative agent for plants.

Keywords:

Arabidopsis thaliana, cell division inhibitor, live-cell imaging, organic chemistry, tobacco BY-2 cell, triarylmethane

Introduction

Proper control of plant cell proliferation is important for various agricultural purposes. In particular, accurate tools to inhibit cell division are crucial to avoid overgrowth after the proper harvest time and to confer dormancy during severe growth conditions. Such tools are also needed by basic researchers to analyze the spatiotemporal control of various division events. However, it is difficult to rapidly and temporally arrest cell division without causing damage. For example, microtubule inhibitors, such as oryzalin, propyzamide and colchicine, effectively inhibit cell division in diverse plant species, but only prevent DNA separation in the M phase of the cell cycle without blocking DNA synthesis in the S phase, and thus generate polyploid cells (Akashi et al. 1988, Liu et al. 1995, Eigsti 1938, Kermani et al. 2003, Grandjean et al. 2004, reviewed in Planchais et al. 2000). In addition, these agents disrupt the organization of cortical microtubules, resulting in abnormal cell expansion (Nakamura et al. 2004). S phase inhibitors including aphidicolin and hydroxyurea block DNA synthesis, without arresting the cell expansion, resulting in abnormal cell outgrowth (Ishikawa et al. 2011, Planchais et al. 2000). Moreover, these S phase inhibitors are not specific to plant species (Pedrali-Noy

et al. 1981). Cell proliferation is also inhibited by various environmental stresses, such as UV-B irradiation and excess boron, but these stresses induce double-strand DNA breaks, and thus their effects are not reversible (Tuteja et al. 2001, Sakamoto et al. 2011).

In contrast to the poor number of plant-specific cell division inhibitors, various agents have been developed for animal cells as antitumor drugs. A series of potent anticancer compounds belong to the triarylmethane family, which has a backbone consisting of three benzene rings. Organic chemists have created various derivatives of triarylmethanes with characteristic motifs, and found that several compounds effectively arrest cell proliferation in human tumor cells (Al-Qawasmeh et al. 2004, Palchaudhuri et al. 2008). Interestingly, two major triarylmethane agents, *S*-trityl-L-cysteine (STLC) and clotrimazole (CLT), block cell division in different manners; STLC targets kinesin Eg5 and halts cells at M phase, whereas CLT induces G1-specific arrest and also apoptosis by an as yet unidentified mechanism (DeBonis et al. 2004, Al-Qawasmeh et al. 2004, Dothager et al. 2005, Skoufias et al. 2006). Since triarylmethanes have a unique three-dimensional structure (Fig. 1A), which is a basis of their derivatives'

activity on specific biological events (Dothager et al. 2005, DeBonis et al. 2008), triarylmethanes would have a potential to develop a new class of agents to affect the biological aspects, on which no inhibitors have been identified.

The Friedel–Crafts reaction is widely used to synthesize triarylmethane derivatives, but it often suffers from selective synthesis of desired products and a limited scope of substrates (Prakash et al. 2009). To overcome these issues, transition-metal catalyzed cross coupling reactions have been developed; however, additional synthetic steps are required to prepare suitable coupling partners (López-Pérez et al. 2009). Recently, we established a method for modular synthesis of triarylmethanes through sequential arylation catalyzed by palladium catalysis (Fig. 1A; Nambo and Crudden 2014). Through this method, structurally diverse triarylmethanes can be prepared using readily available starting materials in three steps.

In this study, we created various derivatives of the triarylmethane family using our synthetic method, and tested their activities on plant cell proliferation. To assess whether their inhibitory effect was based on cell division arrest, rather than enhanced cell death, we utilized live imaging observation of a tobacco BY-2 (Bright Yellow-2)

cell line (*Nicotiana tabacum*) whose microtubules are fluorescently labeled to visualize cell division. This screening revealed a novel compound, (3-furyl)diphenylmethane, as a rapid and nontoxic inhibitor of cell proliferation, whereas some other derivatives, such as diphenyl(3-hydroxyphenyl)methane, induced cell death. Since (3-furyl)diphenylmethane had no effect on a budding yeast or a human cell strain, animals and plants have different sensitivity to triarylmethyl moieties, although the triarylmethane structure is a potent backbone for cell division inhibitors. This was supported by our finding that (3-furyl)phenylmethane, which lacks a benzene ring, does not have antiproliferative activity.

Results

High-throughput assay of cell division frequency

To establish the method to directly monitor the plant cell proliferation activity, we used live imaging of the tobacco culture cell strain, BY-2. In the dual-color fluorescent line, GTRC, which constitutively expresses the α-tubulin protein fused to a green fluorescent protein (GFP-α-tubulin) and the centromeric histone H3 fused to a red

fluorescent protein (RFP-CenH3), time-sequence observation allowed to visualize the cell division dynamics (Fig. 1B; Kurihara et al. 2008). Given that microtubules temporally accumulate around chromosomes as spindle fibers in M phase, live imaging of GFP-α-tubulin allowed us to visualize the antiproliferative activity (Fig. 1B). This activity was also monitored in the single-color line possessing GFP-α-tubulin (BY-GT16) in the presence of 0.1% of vehicle solvent, dimethylsulfoxide (DMSO) (Fig. 2A; Kumagai et al. 2001). For high-throughput screening, we applied each compound to the cells in a 96-well plate, and performed time-lapse imaging with an automated confocal microscope (Fig. 1C; see Materials and Methods). We set the concentration of each compound to 100 μM in BY-2 media, since conventional inhibitors work at several to tens of micromolar (Yoneda et al. 2007, Planchais et al. 2000), and triarylmethanes consisting benzenes generally have low solubility in water. As a positive control, we used 1 μM of a tubulin polymerization inhibitor, oryzalin, which showed a markedly reduced frequency of spindle fiber-like GFP accumulation but did not affect the fluorescence intensity, confirming the effective inhibition of cell proliferation without reducing cell viability (oryzalin in Fig. 2A). At the beginning (0 hr) of time-lapse

observation, which was approximately at 1 hour after the chemical application, the appearance of dividing cells was already reduced in oryzalin-treated cells, and cell division was continuously blocked even after 8 hours (Fig. 2A; Supplementary Table S1).

We then tested whether the known triarylmethane-based anticancer agents STLC and CLT affected plant cell proliferation. When 100 μM of STLC was applied to our assay system, the appearance of dividing cells was indistinguishable from DMSO (STLC in Fig. 2A; Supplementary Table S1), whereas 100 μM of CLT induced cell death—the fluorescence signals were lost and the cells were browned and shrunken (CLT in Supplementary Fig. S1). Given that STLC is effective in human culture cells even at a 100-times lower concentration (Skoufias et al. 2006; see Fig. 7A), these data showed that animals and plants have different reactivity to triarylmethyl moieties. We also found that cell proliferation was not affected by 100 μM of the plain type of triarylmethane, which consists only of intact benzenes (chem1; triphenylmethane; Supplementary Fig. S1; Supplementary Tables S1 and S2). Therefore, we decided to

create diverse triarylmethane derivatives to find effective antiproliferative agents in plant cells.

Synthesis and screening of various triarylmethane derivatives

We synthesized a series of 47 triarylmethane derivatives that included two intact benzene rings and one specifically modified ring (see the "for the first screen" category in Supplementary Table S2; Supplementary Methods) using the method that we recently developed (Fig. 1A; Nambo and Crudden, 2014). We applied these 47 compounds to our assay system at 100 μM in 0.1% DMSO (Fig. 1C), and found that 38 agents showed no visible effects on cell proliferation and eight compounds caused cell death (e.g. chem13, diphenyl(3-hydroxyphenyl)methane; Fig. 2A, B; listed in Supplementary Table S2). We also found that chem7 ((3-furyl)diphenylmethane) significantly reduced the appearance of dividing cells without affecting the fluorescence intensity (Fig. 2A; Supplementary Table S1). No other derivatives showed such a reduction of cell division frequency (Supplementary Table S2), and the furan unit also worked in a different orientation (chem49 in Supplementary Fig. S1; Supplementary Table S1), showing that

furan has specific antiproliferative activity. In order to determine the minimum effective concentration of chem7, we tested the dilution of 50 and 10 μM, but only the original concentration, 100 μM, showed antiproliferative activity ("Dilution" in Supplementary Table S1). Therefore we decided to use 100 μM for further analyses.

Dissection of the structural significance of (3-furyl)diphenylmethane

To investigate the importance of the triarylmethane structure and furan moiety for the antiproliferative effect, we modified each of them (see the "for the second screen" category in Supplementary Table S2). First, we synthesized chem50 and 51, which lacked one benzene ring from chem7, and found that both lost the furan-dependent antiproliferative effect (Fig. 3A; Supplementary Tables S1 and S2). In contrast, chem52 (bis(3-furyl)phenylmethane), which harbored two furan units in the triarylmethane structure, caused cell death (Fig. 3A), presumably because of enhanced activity, as CLT also induces apoptosis in human cells when used together with other anticancer agents (Khalid et al. 1999).

We further modified the structure of chem7 (chem53–60 in Supplementary Table S2; Fig. 3B; Supplementary Fig. S1), and found that the antiproliferative effect was lost when some substituents were installed on the benzene ring (chem54 and 55, compare with chem53; Supplementary Tables S1 and S2; Supplementary Fig. S1), suggesting that the electronic and steric properties of the adjacent benzene ring might be important for access to the target protein. We also synthesized chem56–60, which had chemically more stable furan derivatives than the intact furan, and found that all of them failed to inhibit cell division (Fig. 3C; Supplementary Tables S1 and S2). Given that it has been reported that furan is recognized by cytochrome P450 in human cells and metabolically opened by oxidation (Kobayashi et al. 1987, Peterson et al. 2005, Hamberger et al. 2010), the furan unit might be transformed into some species possessing antiproliferative activity in a similar fashion.

Effect on developing organs of *Arabidopsis thaliana*

We further tested whether chem7 could inhibit cell division during plant development by focusing on various organs of *A. thaliana*. At first, we tested early embryogenesis by

using the live-cell imaging system of *in vitro* cultivated ovules, which we recently established (Gooh et al. 2015). As similar to BY-2 assay, the concentration was 100 μM for chem1 and chem7, and 1 μM for oryzalin in 0.1% DMSO. The embryonic nucleus and plasma membrane were labeled in dual-color fluorescent marker, pWOX2::H2B-GFP pWOX2::tdTomato-LTI6b, and the regular cell divisions of embryos were clearly visualized in the control medium (DMSO in Fig. 4A; Supplementary Movie S1; Gooh et al. 2015). Chem1 showed no effect on embryo patterning, as in BY-2, while chem7 immediately arrested cell division as strongly as oryzalin (Fig. 4A; Supplementary Movie S1), showing that chem7 can block the developmental cell proliferation just after the zygotic division.

Next, to analyze the effect on root growth, 5-day-old seedlings were first grown on chemical-free media and then transferred to new media containing 0.1% DMSO and 1 μM oryzalin, 100 μM chem1, chem7, or chem13 to compare the subsequent root elongation (Fig. 4B). The root growth was not inhibited by chem1, but totally arrested by chem7 as strongly as oryzalin and the cell-death-inducing agent, chem13 (Fig. 4B).

Root elongation depends on cell proliferation in the proximal meristem (PM) at the root tip. The PM is defined as the region between the quiescent center and the first elongated cell in the cortex cell file, where transition zone (TZ) starts for cell differentiation (brackets in Fig. 4C; Takatsuka and Umeda 2014). The PM size gradually decreased in the presence of oryzalin (dotted bracket in Fig. 4C), and PMs were totally lost at 5 days after treatment. The cellular arrangement in the PM was disorganized with expanding cells and the generation of dead cells (arrowheads in Fig. 4C). Oryzalin also caused massive nonpolar cell expansion, presumably by inducing polyploidization and disrupting cortical microtubules (Fig. 4C; Kermani et al. 2003, Baskin et al. 1994). In contrast, chem7 affected neither the cellular organization nor the cell morphology, although the cells in PM gradually elongated and thus shifted into TZ (Fig. 4C, D). This showed that chem7 blocked cell proliferation, but not cell differentiation and elongation, although chem7 did not cause abnormal cell expansion unlike oryzalin. Note that at 5 days after the treatment, the roots had totally stopped growing (Fig. 4B) but the cellular arrangement in PM was unaffected, rarely having dead cells (arrowhead in Fig. 4C).

Furthermore, we also found that chem7 reduced the size of leaves and rosettes at a similar level to oryzalin (Supplementary Fig. S2). Taken all together, we concluded that chem7 can block cell proliferation regardless of tissues and organs.

Cell cycle-independent blocking of cell proliferation

The proliferation arrest without affecting cell morphology implied that chem7 might rapidly inhibit cell division regardless of the cell cycle stage, in contrast to oryzalin, which inhibits M phase but not S phase, and thus induces polyploidization (Kermani et al. 2003). To test this idea, we analyzed the cell cycle state after agent application, using *A. thaliana* that expresses both the M phase-specific cyclin B marker (pCYCB1;2::CYCB1;2-YFP) and the S/G2 phase-specific CDT1a marker (pHTR2::CDT1a (C3)-RFP) (Iwata et al. 2011, Yin et al. 2014). In the root tip, YFP-positive cells were abundant in the PM, marking cells at M phase in the mitotic cycle (DMSO in Fig. 5; Iwata et al. 2011). On the other hand, RFP-positive cells were observed over the entire region, representing cells at S/G2 phase in the mitotic cycle and also the endocycle, where the S phase is repeated and the M phase is skipped to increase

DNA ploidy in differentiated cells (Fig. 5; De Veylder et al. 2007, Edgar et al. 2014, Takatsuka and Umeda 2014, Yin et al. 2014). Neither fluorescence pattern was affected by the negative control, chem1 (Fig. 5). In oryzalin-treated roots, YFP-expressing cells increased but RFP-positive cells decreased, suggesting M phase arrest (Fig. 5). This was consistent with the fact that oryzalin inhibits chromosome alignment, and thus cells are arrested at the spindle assembly checkpoint in the prometaphase-like stage (Yu et al. 1999). Finally, oryzalin caused the loss of fluorescent-positive cells at 5 days after application, suggesting that these abnormally expanded cells were dying (Fig. 5). In contrast, the application of chem7 just gradually reduced the size of the YFP-abundant region while retaining both colors even at 5 days after application, consistent with the gradual reduction of PM size (Fig. 5, compare with Fig. 4C). Therefore, we concluded that the antiproliferative effect of chem7 was independent of cell cycle stage.

Plasticity of the antiproliferative effect

The absence of secondary defects caused by chem7 on cell morphology and viability raised the possibility that cell division could be restarted after removal of the compound.

To test this idea, we first incubated BY-GT16 for 8 hours with different compounds, and then washed them out to perform live imaging (Fig. 6A). The cell division frequency increased after the removal of chem7, but not after removal of chem13, as the cells were already dead, or oryzalin, as the cells were round and expanded (Fig. 6A, compare with Fig. 2A; Supplementary Table S1). A similar result was obtained using roots of *A. thaliana* when 5-day-old seedlings were grown on chemical-containing medium for 2 days and then transferred to a new medium that did not contain the agents (Fig. 6B). The roots gradually restarted their elongation after rescue from chem7-containing medium, and the root length at 3 days after the rescue was significantly greater than in seedlings transferred from oryzalin- or chem13-containing media, although the root was still shorter than DMSO- or chem1-treated roots (Fig. 6B). These results indicated that chem7 was partially reversible.

Effects on other species

In order to assess whether chem7 is a plant-specific antiproliferative inhibitor or also acts on animal cells, we utilized HeLa.S-Fucci2, a human cervical cancer cell line

expressing a fluorescent cell cycle marker (Fluorescent Ubiqutination-based Cell Cycle Indicator; Sakaue-Sawano et al. 2011). We cultured the cells in the presence of STLC, chem1 or chem7 at 1, 10, or 100 μM in 0.2% DMSO for 2 days and tested their effects on cell proliferation using a MTS assay that quantifies living cells (Cory et al. 1991). STLC severely affected cellular viability even at 1 μM (Fig. 7A). On the contrary, chem7 had no effect at 1 or 10 μM, and had only a mild effect at 100 μM, which was comparable to chem1 (Fig. 7A). We also investigated the effect of these chemicals on cell cycle progression. Fucci2 is a genetically encoded cell cycle indicator composed of two chimeric fluorescent proteins, mCherry-hCdt1 and mVenus-hGem (Sakaue-Sawano et al. 2011). Reciprocal accumulation of these two proteins turns cell nuclei red in G1 phase and green in the S/G2/M phases (Sakaue-Sawano et al. 2011). We added compounds to the cell culture at the indicated concentrations and performed time-lapse imaging (Fig. 7B). In the presence of 1 μM STLC, we observed the accumulation of round-shaped cells that emitted green fluorescence followed by cell death (arrowhead in Fig. 7B). These results suggested that STLC blocks the cell cycle in the M phase, which is consistent with a previous report (Skoufias et al. 2006). In contrast, no obvious

differences in cell cycle progression were observed between cells treated with DMSO and 100 μM of chem7 (Fig. 7B), and the proliferation of chem7-treated cells was not reduced compared to DMSO-treated cells (Supplementary Table S3).

We also tested a budding yeast (*Saccharomyces cerevisiae*). Live imaging showed logarithmic growth in the presence of DMSO or 100 μM chem1, and similar proliferation was observed when 100 μM chem7 was present (Supplementary Fig. S3). In contrast, this proliferation was inhibited by 100 μM chem13, although cell morphology was not markedly affected (Supplementary Fig. S3). Chem13 induced cell death in BY-GT16 (and presumably also in *A. thaliana*), suggesting that triarylmethane derivatives have different roles in different species.

Taken together, our results suggested that chem7 might inhibit mechanisms specific to plant species.

Discussion

Biological screening based on desired chemical synthesis

In the past decade, chemical genetic screening has appeared as a powerful tool to study biological mechanisms, instead of genetic screening based on random mutations in the genome (Spring, 2005). In conventional chemical genetic screening, commercially available libraries including diverse compounds are utilized to identify specific molecules that can cause an expected phenotype (Irwin 2006, Yoneda et al. 2007). In contrast, we focused on a unique structure, triarylmethane, some derivatives of which inhibit crucial events of animal cell division, and created various derivatives ourselves. By the first screen utilizing the time-lapse imaging of tobacco cell culture, the novel inhibitor (3-furyl)diphenylmethane (chem7) was identified, and we further synthesized new molecules to identify which chemical properties were necessary for its antiproliferative activity. This is the advantage of combining desired chemical synthesis and direct observation of cell proliferation. We hope that this work will be a new example of the combinational research of synthetic organic chemistry and live-cell imaging to identify specific inhibitors. In addition, we also combined the analysis of

various organs and species, including not only plants, such as tobacco and *A. thaliana*, but also human and yeast, which enabled us to identify the specific effect of (3-furyl)diphenylmethane on the cell proliferation of plants.

The role of (3-furyl)diphenylmethane in cell proliferation

We found that (3-furyl)diphenylmethane worked regardless of the cell cycle stage and did not have severe effects on cell size, viability, or pattern formation. These features, together with reversibility, are beneficial for the use of this agent as an effective and temporary cell division inhibitor. So far the minimum effective concentration of (3-furyl)diphenylmethane is 100 μM, which is relatively high to use as a conventional agent, and thus further structural modification to improve water solubility will be needed to minimize the effective dose of (3-furyl)diphenylmethane.

It is also important to identify the target of (3-furyl)diphenylmethane to understand its inhibitory mechanism. One possible candidate for the target protein might be a kinesin, since STLC directly binds to the catalytic domain of a human kinesin, Eg5 (Skoufias et al. 2006). However, this is unlikely because STLC itself did not affect the cell

proliferation of BY-2 even at a 100-times higher concentration than the effective concentration in human cells, and all known kinesins in *A. thaliana* (61 genes) are predicted to function in microtubule-related regulation, such as spindle assembly and the formation of the preprophase band at M phase (reviewed in Zhu and Dixit, 2012). Therefore this idea cannot explain the different effects of (3-furyl)diphenylmethane from the strong microtubule inhibitor, oryzalin.

Another candidate might be some regulator of the production and/or uptake of essential nutrients, such as sucrose, nitrogen, and phosphate. For example, phosphate starvation increases sensitivity to the plant hormone auxin in the root meristem to halt cell proliferation (López-Bucio et al. 2002, Pérez-Torres et al. 2008). This idea would explain that the cell proliferation activity was partially restored after (3-furyl)diphenylmethane was washed out, as plants can restart the growth after starvation ends. The fact that the cell proliferation was not fully restored after the removal of (3-furyl)diphenylmethane suggests the possibility that this compound has a potential reactivity causing irreversible cell damage or that the excessive cell differentiation exhausts the proliferating cells as the PM was reduced in roots.

Identification of the (3-furyl)diphenylmethane target would show us the exact inhibition mechanism of plant cell proliferation.

How can we identify the target protein? Given that the usual triarylmethane contains two intact benzenes and one specifically modified benzene ring, we predict that binding would occur as follows: the two hydrophobic benzenes bind to hydrophobic residues surrounding the core catalytic site of the target protein to stably hold the compound, and the specific benzene ring perturbs the core site. This idea is supported by our findings that the two intact benzenes are both required for the antiproliferative activity of (3-furyl)diphenylmethane. Our finding that the inhibitory effect was lost by stabilizing the furan unit might imply that this unit is metabolically modified to an active form, similarly to the known metabolic pathway of cytochrome P450 that opens the furan ring (Kobayashi et al. 1987, Hamberger et al. 2010). Therefore, a plausible way of identifying the target would be conjugating a PEG chain at the benzene junction of (3-furyl)diphenylmethane to leave all rings intact and to connect this compound to a protein adhesion column to collect the target proteins from a crude extract of BY-2 cells (reviewed in Ziegler et al. 2013).

Materials and Methods

General procedure for synthesis of triarylmethane derivatives

A 10 mL sealable glass vessel containing a magnetic stirring bar was flame-dried under a vacuum and filled with argon after cooling to room temperature. In the case of chem13, allylpalladium chloride dimer (1.8 mg, 5 μmol), 1,3-bis(2,6-diisopropylphenyl)imidazolinium chloride (4.3 mg, 10 μmol), dry dioxane (0.25 mL), and 1 M NaOH*aq* (0.3 mL, 0.3 mmol) were added to the glass vessel at room temperature under a stream of argon. After stirring the mixture at this temperature for 30 min, diphenylmethyl phenyl sulfone (30.8 mg, 0.1 mmol), *3*-hydroxyphenylboronic acid (27.6 mg, 0.2 mmol), and dry dioxane (0.25 mL) were added, and then the vessel was sealed. The mixture was stirred at 120 °C for 12 hours. After cooling to room temperature, the mixture was passed through a pad of silica gel with copious washings with EtOAc (~15 mL). The filtrate was concentrated under reduced pressure. The crude product was purified by PTLC (hexane:EtOAc = 10:1) to give diphenyl(3-hydroxyphenyl)methane (chem13, 12.2 mg, 47%) as a white solid. The

method used to synthesize other compounds is described in Supplementary Methods and is also available upon request. Detailed methods and data sets of each product, such as ^{1}H and ^{13}C NMR spectra, are also shown in Supplementary Methods.

Strains and growth conditions

All strains of *Arabidopsis thaliana* were in Columbia background. *A. thaliana* was grown in Petri dishes containing 1.5% agar medium and 1/2 Murashige and Skoog (MS) medium, or on soil under continuous light at 18–22°C. The HeLa.S-Fucci2 cell line was provided by RIKEN BRC. Cells were cultured under 5% CO_2 at 37°C in Dulbecco's modified Eagle medium (DMEM) supplemented with 10% fetal calf serum (FCS), 100 units/mL penicillin and 100 mg/mL streptomycin. The budding yeast strain AH109 was grown according to the Yeast Handbook (Clontech, https://www.clontech.com). Tobacco BY-GT16 and BY-GTRC cells were maintained as previously described (Kumagai et al. 2001, Kurihara et al. 2008). pWOX2::H2B-GFP and pWOX2::tdTomato-LTI6b were described previously (Gooh et al. 2015).

pCYCB1;2::CYCB1;2-YFP and pHTR2::CDT1a (C3)-RFP were also described previously (Iwata et al. 2011, Yin et al. 2014).

Live imaging and screening

For time-lapse imaging of BY-GTRC and BY-GT16 strains, 3- or 4-day-old cell culture were used. The BY-GTRC cells were mounted on a cover slip with a gas-permeable sheet (Opticell; Nunc, http://www.thermofisher.com/). The BY-GT16 cells were diluted in the culture media to 1/10~1/20, and 1 mL of the diluted cells were mixed with 1 μL of stock solution of each chemical compound (100 mM of triarylmethane derivatives or 1 mM of oryzalin in 100% DMSO); i.e. the final concentration is 100 μM triarylmethane derivatives or 1 μM oryzalin with 0.1% DMSO. The 100 μL of the mixed cell was transferred into a 96-well glass bottom plate (Greiner, http://www.greinerbioone.com/), and time-lapse imaging was started (0 hr) at approximately 1 hour after the chemical mixing.

Time-lapse imaging was performed using an inverted confocal microscope system with a stable incubation chamber (CV1000; Yokogawa Electric, http://www.yokogawa.com)

equipped with 488-nm and 561-nm lasers (Yokogawa Electric) and EMCCD camera (ImagEM C9100-13; Hamamatsu Photonics, http://www.hamamatsu.com/jp/en/index.html). Images of BY-GTRC were acquired using a 40× objective lens (40x UPLSAPO, NA = 0.95; Olympus, http://www.olympus-global.com/en/network/) at 7 z-stacks with 5-μm intervals every 10 min for 24 hours. Images of BY-GT16 were collected using a 10× objective lens (10× UPLSAPO, NA = 0.40; Olympus) at 10 z-stacks with 10-μm intervals every 10 min for 24 hours. We used the band-pass filters of 520/35 nm for GFP and 617/73 nm for RFP, and two positions in two replicates were observed for each compound. To test the agent removability, BY-GT16 was incubated with each compound for 8 hours without imaging, and then the medium was replaced with a fresh medium for time-lapse imaging as above.

Live imaging of *A. thaliana* embryogenesis was performed using *in vitro* ovule cultivation method (Gooh et al. 2015), except for the microscope system, where the CV1000 was used with a 40× objective lens.

For live imaging of yeast cells, an overnight culture was 100-fold-diluted and placed in the CV1000 using a similar setting to BY-GT16 but with a 40× objective lens.

For live imaging of the HeLa.S-Fucci2 cell line, cells were plated onto a 96-well glass bottom plate at a density of 5×10^3 cells/well. After 24 hours of culture, compounds were added to the cells and they were placed in the CV1000. Images were acquired every 30 min with a 40× objective lens under 5% CO_2 at 37°C. mCherry-hCdt1 and mVenus-hGem were excited by 488- and 561-nm laser lines, respectively. We used two band-pass filters of 520/35 nm for mVenus and 617/73 nm for mCherry.

Same stock solutions were used for all assays, and thus the final concentration of DMSO was always 0.1%, only except for the human cell assays, where cultures were treated with 500-fold concentrated stocks dissolved in 100% DMSO, and thus the final concentration of DMSO in the culture media was 0.2%. For dilution series experiments, the stock solutions were at first diluted in 100% DMSO, and they were used as 1000-fold stock solution for each dilution series (i.e. the final concentration of DMSO was 0.1%).

Histological analysis

To examine the cell arrangement in the root, root tips were stained with 10 μg/mL PI solution (Sigma, http://www.sigmaaldrich.com/sigma-aldrich/home.html) and observed using a confocal laser-scanning microscope (LSM780; Carl Zeiss, http://www.zeiss.com/microscopy/en_de/home.html) with a 20× objective lens (20× Plan-APOCHROMAT, NA = 0.80; Zeiss). The PI emission signal was detected between 560 and 735 nm with 561-nm excitation. LSM780 was also used to observe roots expressing pCYCB1;2::CYCB1;2-YFP and pHTR2::CDT1a (C3)-RFP. The emission signal of YFP was detected between 491 and 558 nm with 488-nm excitation, and that of RFP was detected between 570 and 649 nm with 561-nm excitation. The length of *A. thaliana* roots was measured with the MBF ImageJ software.

MTS assay for cell viability

HeLa.S-Fucci2 cells were plated onto clear 96-well plates at a density of 8×10^2 cells/well and cultured in DMEM supplemented with 10% FCS. After 24 hours of culture, compounds were added with the cells at the concentrations indicated in Fig. 7A,

and incubated further for two days. DMSO was used as a vehicle in this experiment, the concentration of which was 0.2%. MTS assay was performed using the CellTiter 96 AQueous One Solution Cell Proliferation Assay (Promega, http://www.promega.com/) according to the manufacturer's instructions. Briefly, 20 μL of MTS solution was added to each well containing 100 μL of medium and incubated for 1 hour at 37°C. Absorbance at 490 nm was monitored by a microplate reader.

Funding

This work was supported by an ITbM Research Award from ITbM. JSPS and Nagoya University are acknowledged for funding of this research through The World Premier International Research Center Initiative (WPI) program. M.Ueda was supported by the Japan Society for the Promotion of Science (Grant-in-Aid for Scientific Research on Innovative Areas (No. 24113514, 26113710, and 15H05962), a Grant-in-Aid for Young Scientists (B, No. 24770045 and 26840093), a Grant-in-Aid for challenging Exploratory Research (No. 16K14753) and JST, ERATO (No. 25-J-J4216). M.N. was supported by

a Grant-in-Aid for Young Scientists (B, No. 26810056). T.O. was supported by a Grand-in-Aid for Exploratory Research (No. 26650033).

Disclosures

The authors have no conflicts of interest to declare.

Acknowledgements

We thank Cathleen M. Crudden, Kenichiro Itami, Tetsuya Higashiyama, and Takashi Yoshimura for helpful discussions, Masaki Ito for pCYCB1;2::CYCB1;2-YFP, and RIKEN BRC for BY-GT16 and HeLa.S-Fucci2.

References

Akashi, T., Izumi, K., Nagano, E., Enomoto, M., Mizuno, K. and Shibaoka, H. (1988) Effects of Propyzamide on Tobacco Cell Microtubules In Vivo and In Vitro. *Plant & cell physiology* 29: 1053-1062.

Al-Qawasmeh, R.A., Lee, Y., Cao, M.Y., Gu, X., Vassilakos, A., Wright, J.A., et al. (2004) Triaryl methane derivatives as antiproliferative agents. *Bioorganic & medicinal chemistry letters* 14: 347-350.

Baskin, T.I., Wilson, J.E., Cork, A. and Williamson, R.E. (1994) Morphology and microtubule organization in Arabidopsis roots exposed to oryzalin or taxol. *Plant & cell physiology* 35: 935-942.

Cory, A.H., Owen, T.C., Barltrop, J.A. and Cory, J.G. (1991) Use of an aqueous soluble tetrazolium/formazan assay for cell growth assays in culture. *Cancer Commun* 3: 207-212.

De Veylder, L., Beeckman, T. and Inze, D. (2007) The ins and outs of the plant cell cycle. *Nature reviews. Molecular cell biology* 8: 655-665.

DeBonis, S., Skoufias, D.A., Indorato, R.L., Liger, F., Marquet, B., Laggner, C., et al. (2008) Structure-activity relationship of S-trityl-L-cysteine analogues as inhibitors of the human mitotic kinesin Eg5. *Journal of medicinal chemistry* 51: 1115-1125.

DeBonis, S., Skoufias, D.A., Lebeau, L., Lopez, R., Robin, G., Margolis, R.L., et al. (2004) In vitro screening for inhibitors of the human mitotic kinesin Eg5 with antimitotic and antitumor activities. *Molecular cancer therapeutics* 3: 1079-1090.

Dothager, R.S., Putt, K.S., Allen, B.J., Leslie, B.J., Nesterenko, V. and Hergenrother, P.J. (2005) Synthesis and identification of small molecules that potently induce apoptosis in melanoma cells through G1 cell cycle arrest. *Journal of the American Chemical Society* 127: 8686-8696.

Edgar, B.A., Zielke, N. and Gutierrez, C. (2014) Endocycles: a recurrent evolutionary innovation for post-mitotic cell growth. *Nature reviews. Molecular cell biology* 15: 197-210.

Eigsti, O.J. (1938) A Cytological Study of Colchicine Effects in the Induction of Polyploidy in Plants. *Proceedings of the National Academy of Sciences of the United States of America* 24: 56-63.

Gooh, K., Ueda, M., Aruga, K., Park, J., Arata, H., Higashiyama, T., et al. (2015) Live-Cell Imaging and Optical Manipulation of Arabidopsis Early Embryogenesis. *Developmental cell* 34: 242-251.

Grandjean, O., Vernoux, T., Laufs, P., Belcram, K., Mizukami, Y. and Traas, J. (2004) In vivo analysis of cell division, cell growth, and differentiation at the shoot apical meristem in Arabidopsis. *The Plant cell* 16: 74-87.

Hamberger, C., Kellert, M., Schauer, U.M., Dekant, W. and Mally, A. (2010) Hepatobiliary toxicity of furan: identification of furan metabolites in bile of male f344/n rats. *Drug metabolism and disposition: the biological fate of chemicals* 38: 1698-1706.

Irwin, J.J. (2006) How good is your screening library? *Current opinion in chemical biology* 10: 352-356.

Ishikawa, M., Murata, T., Sato, Y., Nishiyama, T., Hiwatashi, Y., Imai, A., et al. (2011) Physcomitrella cyclin-dependent kinase A links cell cycle reactivation to other cellular changes during reprogramming of leaf cells. *The Plant cell* 23: 2924-2938.

Iwata, E., Ikeda, S., Matsunaga, S., Kurata, M., Yoshioka, Y., Criqui, M.C., et al. (2011) GIGAS CELL1, a novel negative regulator of the anaphase-promoting complex/cyclosome, is required for proper mitotic progression and cell fate determination in Arabidopsis. *The Plant cell* 23: 4382-4393.

Kermani, M.J., Sarasan, V., Roberts, A.V., Yokoya, K., Wentworth, J. and Sieber, V.K. (2003) Oryzalin-induced chromosome doubling in Rosa and its effect on plant morphology and pollen viability. *TAG. Theoretical and applied genetics. Theoretische und angewandte Genetik* 107: 1195-1200.

Khalid, M.H., Shibata, S. and Hiura, T. (1999) Effects of clotrimazole on the growth, morphological characteristics, and cisplatin sensitivity of human glioblastoma cells in vitro. *Journal of neurosurgery* 90: 918-927.

Kobayashi, T., Sugihara, J. and Harigaya, S. (1987) Mechanism of metabolic cleavage of a furan ring. *Drug metabolism and disposition: the biological fate of chemicals* 15: 877-881.

Kumagai, F., Yoneda, A., Tomida, T., Sano, T., Nagata, T. and Hasezawa, S. (2001) Fate of nascent microtubules organized at the M/G1 interface, as visualized by synchronized tobacco BY-2 cells stably expressing GFP-tubulin: time-sequence observations of the reorganization of cortical microtubules in living plant cells. *Plant & cell physiology* 42: 723-732.

Kurihara, D., Matsunaga, S., Uchiyama, S. and Fukui, K. (2008) Live cell imaging reveals plant aurora kinase has dual roles during mitosis. *Plant & cell physiology* 49: 1256-1261.

Lopez-Bucio, J., Hernandez-Abreu, E., Sanchez-Calderon, L., Nieto-Jacobo, M.F., Simpson, J. and Herrera-Estrella, L. (2002) Phosphate availability alters architecture and causes changes in hormone sensitivity in the Arabidopsis root system. *Plant physiology* 129: 244-256.

Lopez-Perez, A., Adrio, J. and Carretero, J.C. (2009) Palladium-catalyzed cross-coupling reaction of secondary benzylic bromides with grignard reagents. *Organic Letter.* 11: 5514-5517.

Nakamura, M., Naoi, K., Shoji, T. and Hashimoto, T. (2004) Low concentrations of propyzamide and oryzalin alter microtubule dynamics in Arabidopsis epidermal cells. *Plant & cell physiol.* 45: 1330-1334.

Nambo, M. and Crudden, C.M. (2014) Modular synthesis of triarylmethanes through palladium-catalyzed sequential arylation of methyl phenyl sulfone. *Angewandte Chemie (International edition)* 53: 742-746.

Palchaudhuri, R., Nesterenko, V. and Hergenrother, P.J. (2008) The complex role of the triphenylmethyl motif in anticancer compounds. *Journal of the American Chemical Society* 130: 10274-10281.

Pedrali-Noy, G., Kuenzle, C.C., Focher, F., Belvedere, M. and Spadari, S. (1981) An enzymatic method for microdetermination of aphidicolin: a promising anticancer drug. *Journal of biochemical and biophysical methods* 4: 113-121.

Perez-Torres, C.A., Lopez-Bucio, J., Cruz-Ramirez, A., Ibarra-Laclette, E., Dharmasiri, S., Estelle, M., et al. (2008) Phosphate availability alters lateral root development in Arabidopsis by modulating auxin sensitivity via a mechanism involving the TIR1 auxin receptor. *The Plant cell* 20: 3258-3272.

Peterson, L.A., Cummings, M.E., Vu, C.C. and Matter, B.A. (2005) Glutathione trapping to measure microsomal oxidation of furan to cis-2-butene-1,4-dial. *Drug metabolism and disposition: the biological fate of chemicals* 33: 1453-1458.

Planchais, S., Glab, N., Inze, D. and Bergounioux, C. (2000) Chemical inhibitors: a tool for plant cell cycle studies. *FEBS letters* 476: 78-83.

Prakash, G.K., Panja, C., Shakhmin, A., Shah, E., Mathew, T. and Olah, G.A. (2009) BF3-H2O catalyzed hydroxyalkylation of aromatics with aromatic aldehydes and dicarboxaldehydes: efficient synthesis of triarylmethanes, diarylmethylbenzaldehydes, and anthracene derivatives. *Journal of Organic Chemistry* 74: 8659-8668.

Sakamoto, T., Inui, Y.T., Uraguchi, S., Yoshizumi, T., Matsunaga, S., Mastui, M., et al. (2011) Condensin II alleviates DNA damage and is essential for tolerance of boron overload stress in Arabidopsis. *The Plant cell* 23: 3533-3546.

Sakaue-Sawano, A., Kobayashi, T., Ohtawa, K. and Miyawaki, A. (2011) Drug-induced cell cycle modulation leading to cell-cycle arrest, nuclear mis-segregation, or endoreplication. *BMC cell biology* 12: 2.

Skoufias, D.A., DeBonis, S., Saoudi, Y., Lebeau, L., Crevel, I., Cross, R., et al. (2006) S-trityl-L-cysteine is a reversible, tight binding inhibitor of the human kinesin Eg5 that specifically blocks mitotic progression. *The Journal of biological chemistry* 281: 17559-17569.

Spring, D.R. (2005) Chemical genetics to chemical genomics: small molecules offer big insights. *Chemical Society Reviews* 34: 472-482.

Takatsuka, H. and Umeda, M. (2014) Hormonal control of cell division and elongation along differentiation trajectories in roots. *Journal of experimental botany* 65: 2633-2643.

Tuteja, N., Singh, M.B., Misra, M.K., Bhalla, P.L. and Tuteja, R. (2001) Molecular mechanisms of DNA damage and repair: progress in plants. *Critical reviews in biochemistry and molecular biology* 36: 337-397.

Yin, K., Ueda, M., Takagi, H., Kajihara, T., Sugamata Aki, S., Nobusawa, T., et al. (2014) A dual-color marker system for in vivo visualization of cell cycle progression in Arabidopsis. *The Plant journal : for cell and molecular biology* 80: 541-552.

Yoneda, A., Higaki, T., Kutsuna, N., Kondo, Y., Osada, H., Hasezawa, S., et al. (2007) Chemical genetic screening identifies a novel inhibitor of parallel alignment of cortical microtubules and cellulose microfibrils. *Plant & cell physiology* 48: 1393-1403.

Yu, H.G., Muszynski, M.G. and Kelly Dawe, R. (1999) The maize homologue of the cell cycle checkpoint protein MAD2 reveals kinetochore substructure and contrasting mitotic and meiotic localization patterns. *The Journal of cell biology* 145: 425-435.

Zhu, C. and Dixit, R. (2012) Functions of the Arabidopsis kinesin superfamily of microtubule-based motor proteins. *Protoplasma* 249: 887-899.

Ziegler, S., Pries, V., Hedberg, C. and Waldmann, H. (2013) Target identification for small bioactive molecules: finding the needle in the haystack. *Angewandte Chemie (International ed. in English)* 52: 2744-2792.

Legends to figures

Fig. 1 Combination of synthetic chemistry and live-cell imaging to create novel drugs that affect plant cell proliferation.

(A) Schematic procedure of modular synthesis of triarylmethane derivatives. Two sequential C–H arylations and a desulfonative Suzuki–Miyaura cross coupling convert methyl phenyl sulfone to triarylmethanes. (B) Time-sequence observation of the cell division behavior of BY-GTRC. Arrowheads indicate spindle formation in dividing cells. Numbers indicate the time (hr: min) from the first frame. GFP- α -tubulin (green) and RFP-CenH3 (magenta) are merged. (C) Schematic procedure of the screening. Each triarylmethane derivative was mixed with fluorescently labeled BY-2 cells in a 96-well glass bottom plate, and time-lapse imaging was performed with an automated confocal microscope to screen the compounds that affect cell proliferation activity.

Scale bar, 40 μm.

Fig. 2 (3-Furyl)diphenylmethane was identified as a cell division inhibitor among newly generated triarylmethane derivatives.

(A) Time-sequence observation of the cell division behavior of BY-GT16 (BY-2 cells expressing p35S::GFP- α -tubulin) in the presence of the indicated compounds. Arrowheads show dividing cells, which formed spindles at the respective timing, and actually divided in the later time frames. The right panels are merged GFP and bright field images showing cell viability. (B) Structure of triarylmethane derivatives. Various functional groups were placed at the Ar position (green); these derivatives are categorized based on their effects on BY-2 cells.

Oryzalin and each triarylmethane derivative were added at 1 and 100 μM, respectively, in 0.1% DMSO. Scale bar, 40 μm.

Fig. 3 Triarylmethane structure, adjacent benzene rings, and reactive furan unit are all crucial for antiproliferative activity.

(A, C) Time-sequence observation of the cell division behavior of BY-GT16 in the presence of the indicated compounds. Arrowheads show dividing cells. The right panels are merged GFP and bright field images. (B) Structure of triarylmethane derivatives

containing a furan unit. Various functional groups were placed at the Ar position (blue); these derivatives are categorized based on their effects on BY-2 cells.

Each triarylmethane derivative was added at 100 μM in 0.1% DMSO. Scale bars, 40 μm.

Fig. 4 (3-Furyl)diphenylmethane is sufficient to block cell division in various organs of *Arabidopsis thaliana*.

(A) Time-sequence observation of embryogenesis in the presence of the indicated compounds. Nucleus and plasma membrane of the embryos were labeled with pWOX2::H2B-GFP (green) and pWOX2::tdTomato-LTI6b (magenta), respectively.

(B) Root length of *A. thaliana* after the indicated compounds were applied to seedlings 5 days after germination (DAG). Error bars represent SD ($n \geq 19$). The values at 5 days after chemical application were not significantly different between DMSO and chem1, or among oryzalin, chem7 and chem13, but these two groups were significantly different from each other ($P < 0.01$, Tukey-Kramer test). (C) Roots stained with propidium iodide (PI). Roots were observed on the indicated days after the application

of each compound. Solid and dotted brackets show proximal meristems (PMs) and unclear PM regions in chem7- and oryzalin-treated roots, respectively. Arrowheads indicate dead cells, which were fully stained by PI. (D) Cell number in PMs of (C) at 1 and 2 days after application of the indicated compounds. Error bars represent SD (n = 2). Significant difference from the value of DMSO-treated roots was determined by the Dunnett's test ($P < 0.01$ (**) or $P < 0.05$ (*)) in (D). Ns, not significant. Note that cell number was not counted in oryzalin-treated roots, since the region of PM was unclear as shown in (C).

Oryzalin, chem1 and chem7 were added at 1, 100 and 100 μM, respectively, in 0.1% DMSO. Scale bars, 10 μm (A), and 100 μm (C).

Fig. 5 (3-Furyl)diphenylmethane acts independently of the cell cycle stage.

A. thaliana roots expressing pHTR2::CDT1a (C3)-RFP (magenta) and pCYCB1;2::CYCB1;2-YFP (green), labeling cells in S/G2 and M phase, respectively. Roots were observed on the indicated days after the application of each compound. Brackets show the region where YFP- and RFP-positive cells are both abundant.

Oryzalin, chem1 and chem7 were added at 1, 100 and 100 μM, respectively, in 0.1% DMSO. Scale bar, 100 μm.

Fig. 6 Effect of (3-furyl)diphenylmethane is partially reversible.

(A) Time-sequence observation of BY-GT16 after removal of the indicated compounds following incubation for 8 hours. Arrowheads show dividing cells, and the right panels are merged GFP and bright field images. (B) Root length of *A. thaliana* after removal of the indicated compounds following incubation for 2 days (day −2 and −1). Error bars represent SD ($n \geq 20$). The values at 3 days after removal were not significantly different between DMSO and chem1 or between oryzalin and chem13, but both groups showed significant difference from each other and from chem7 ($P < 0.01$, Tukey-Kramer test).

Oryzalin, chem7 and chem13 were added at 1, 100 and 100 μM, respectively, in 0.1% DMSO. Scale bar, 40 μm.

Fig. 7 (3-Furyl)diphenylmethane does not inhibit the growth of human cells.

(A) Viability of HeLa.S-Fucci2 cells accessed by MTS assay. The number of viable cells after 3 days exposure to the indicated compounds is expressed as a percentage of the DMSO-treated control. Error bars represent SD (n = 4). (B) Time-sequence observation of the cell cycle progression of HeLa.S-Fucci2 cells in the presence of the indicated compounds. Red and green fluorescence were emitted from mCherry-hCdt1 (a G1 phase marker) and mVenus-hGem (a marker of the S/G2/M phases), respectively. Yellow and white arrowheads indicate the cells before and after division, respectively Arrows indicate a cell arrested at M phase and then undergoing cell death.

STLC and chem7 were added at 1 and 100 μM, respectively, in 0.2% DMSO. Scale bar, 25 μm.

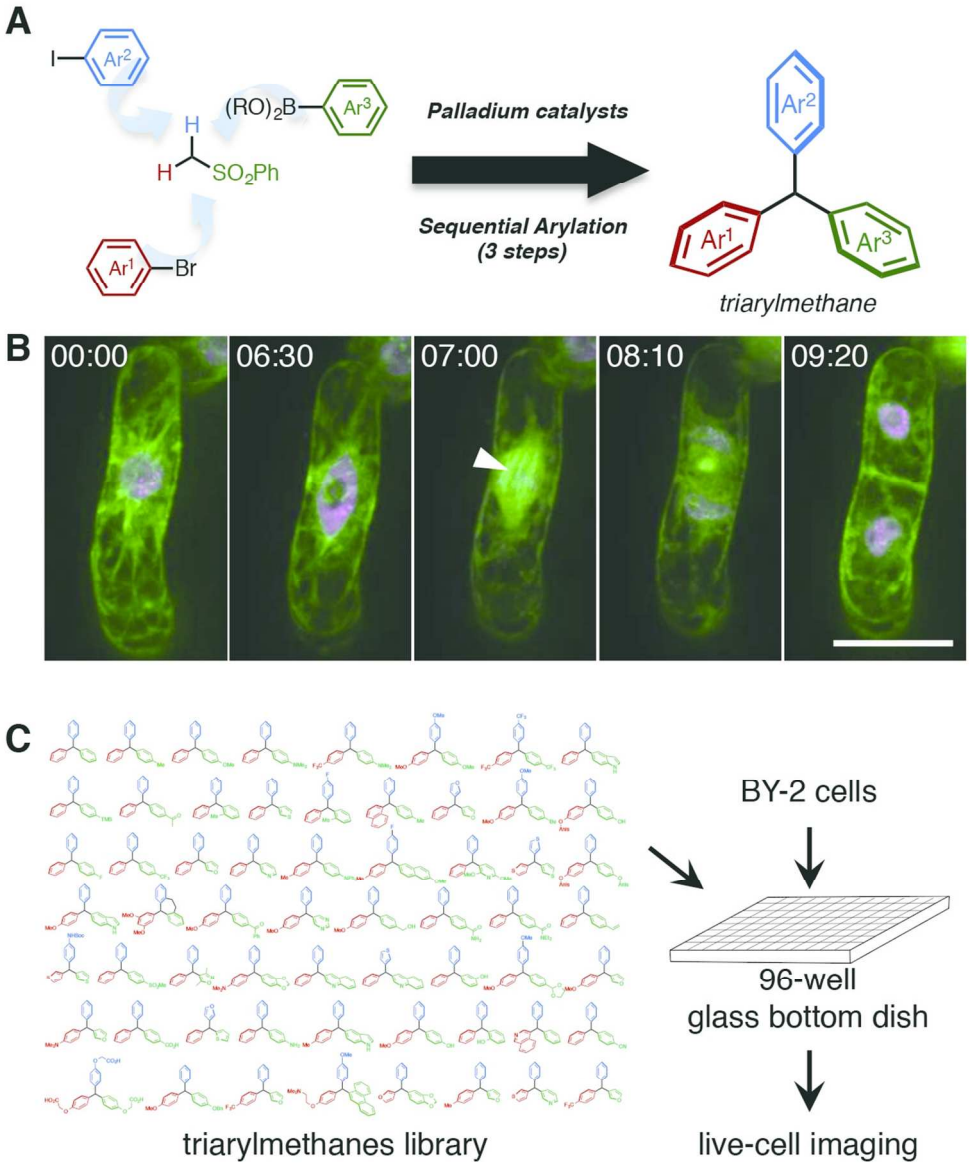

Fig. 1 Combination of synthetic chemistry and live-cell imaging to create novel drugs that affect plant cell proliferation.

113x135mm (300 x 300 DPI)

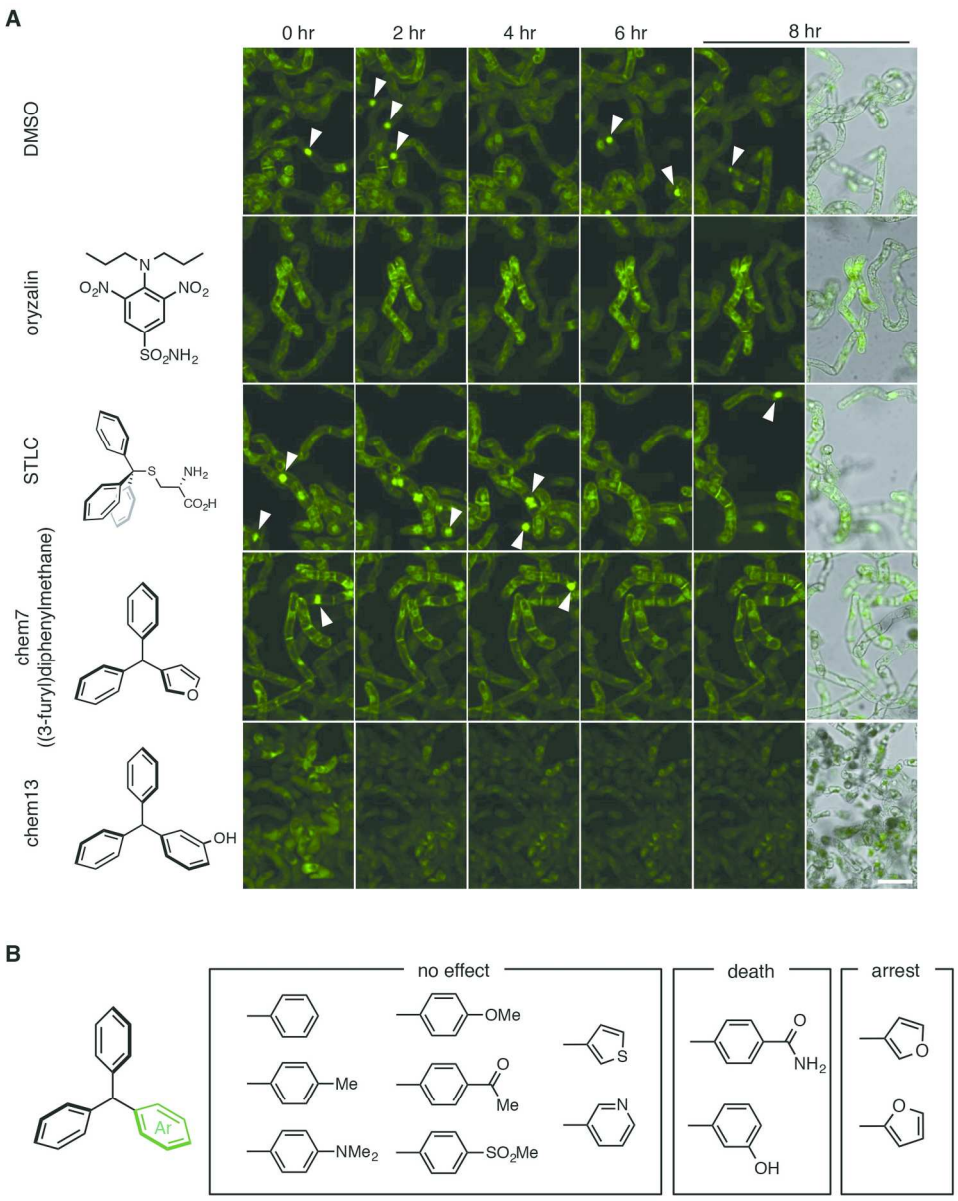

Fig. 2 (3-Furyl)diphenylmethane was identified as a cell division inhibitor among newly generated triarylmethane derivatives.

181x224mm (300 x 300 DPI)

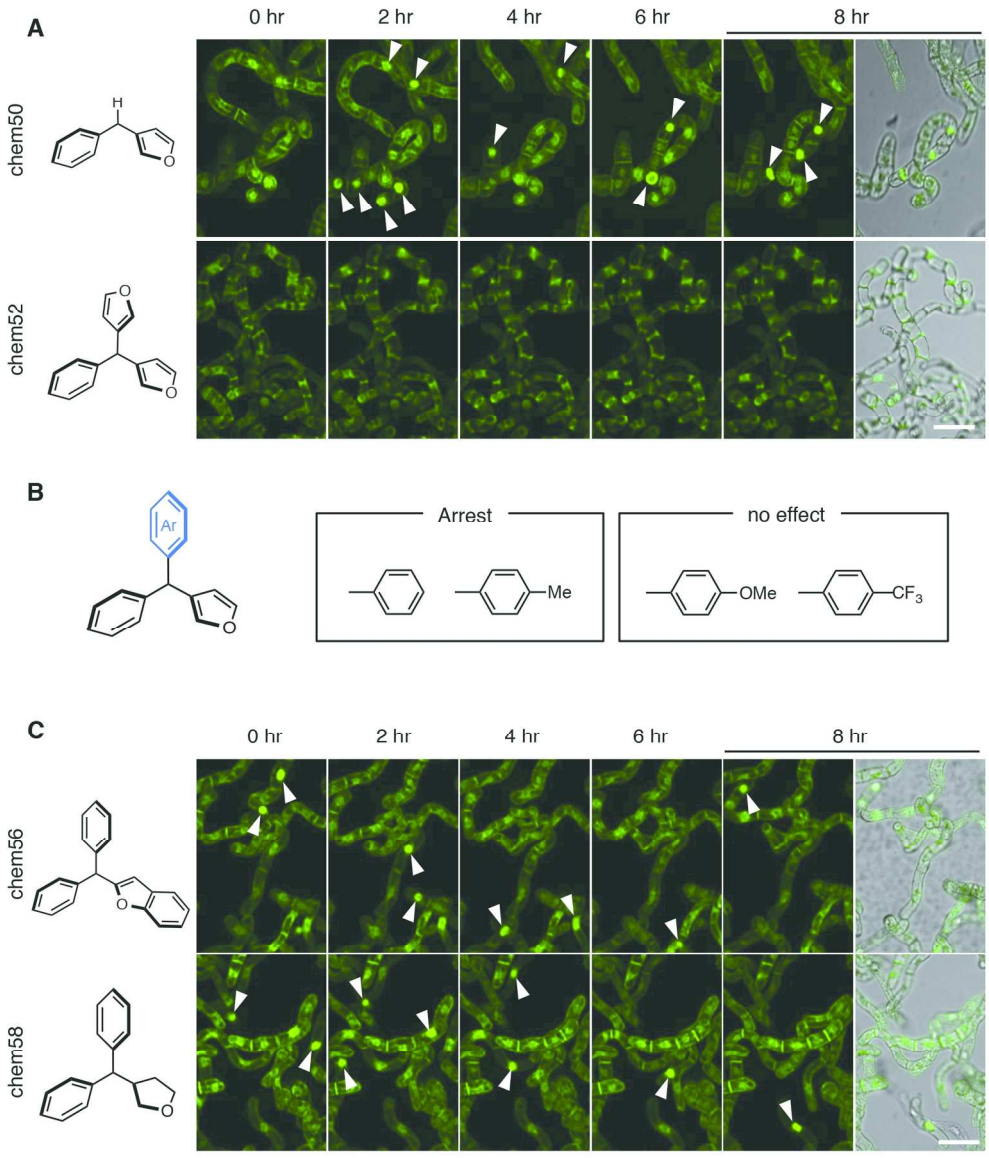

Fig. 3 Triarylmethane structure, adjacent benzene rings, and reactive furan unit are all crucial for antiproliferative activity.

173x201mm (300 x 300 DPI)

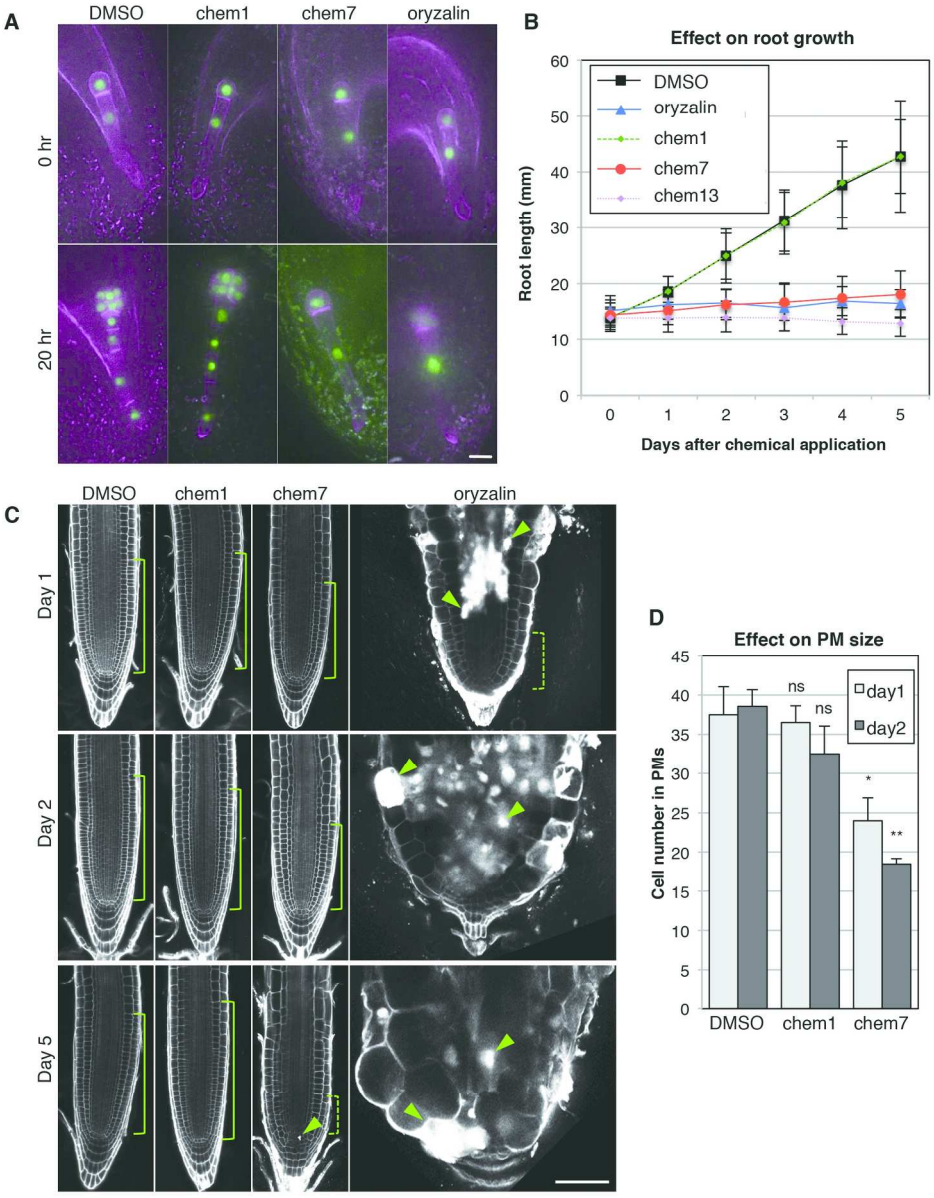

Fig. 4 (3-Furyl)diphenylmethane is sufficient to block cell division in various organs of Arabidopsis thaliana.

183x232mm (300 x 300 DPI)

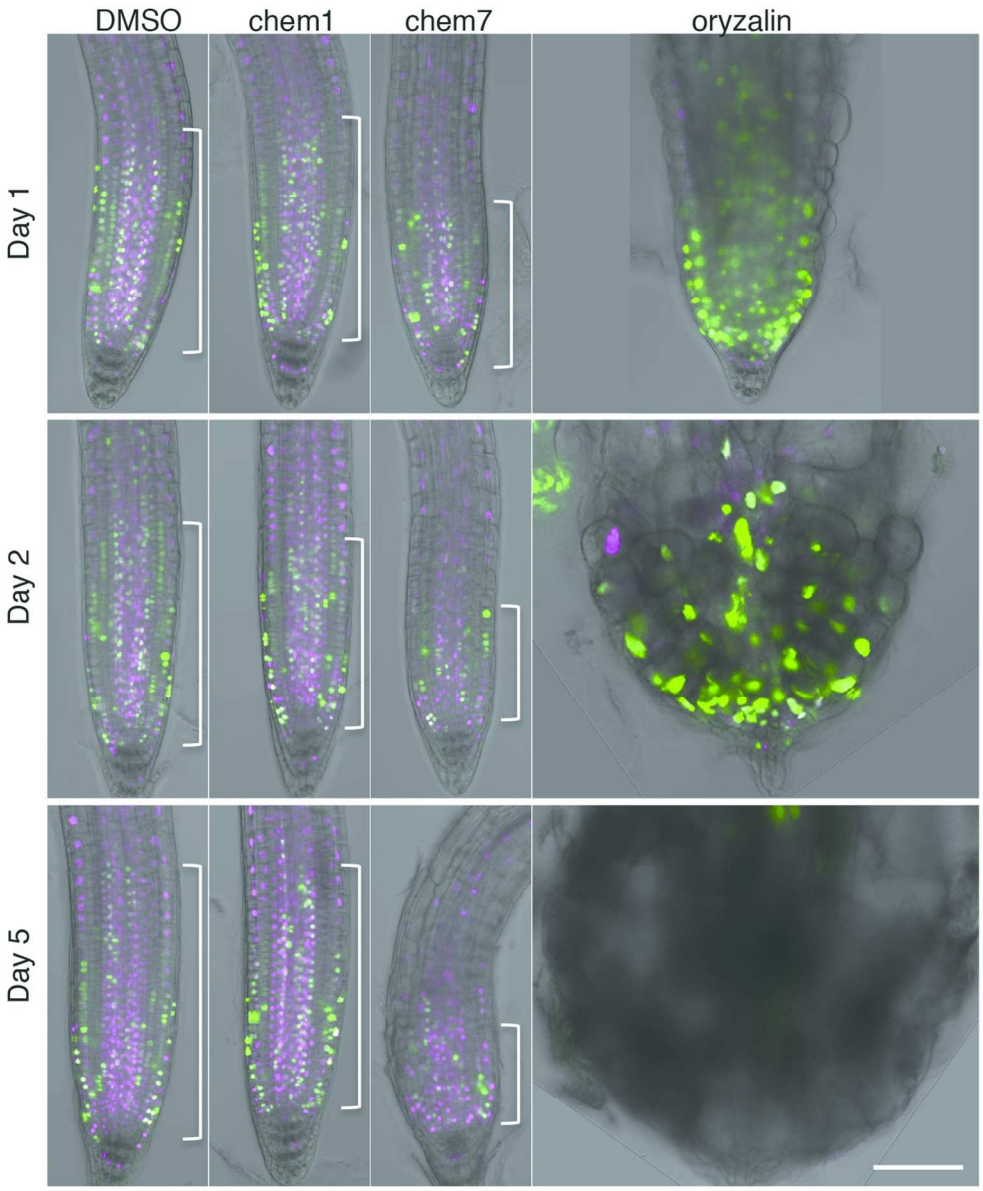

Fig. 5 (3-Furyl)diphenylmethane acts independently of the cell cycle stage.

120x144mm (300 x 300 DPI)

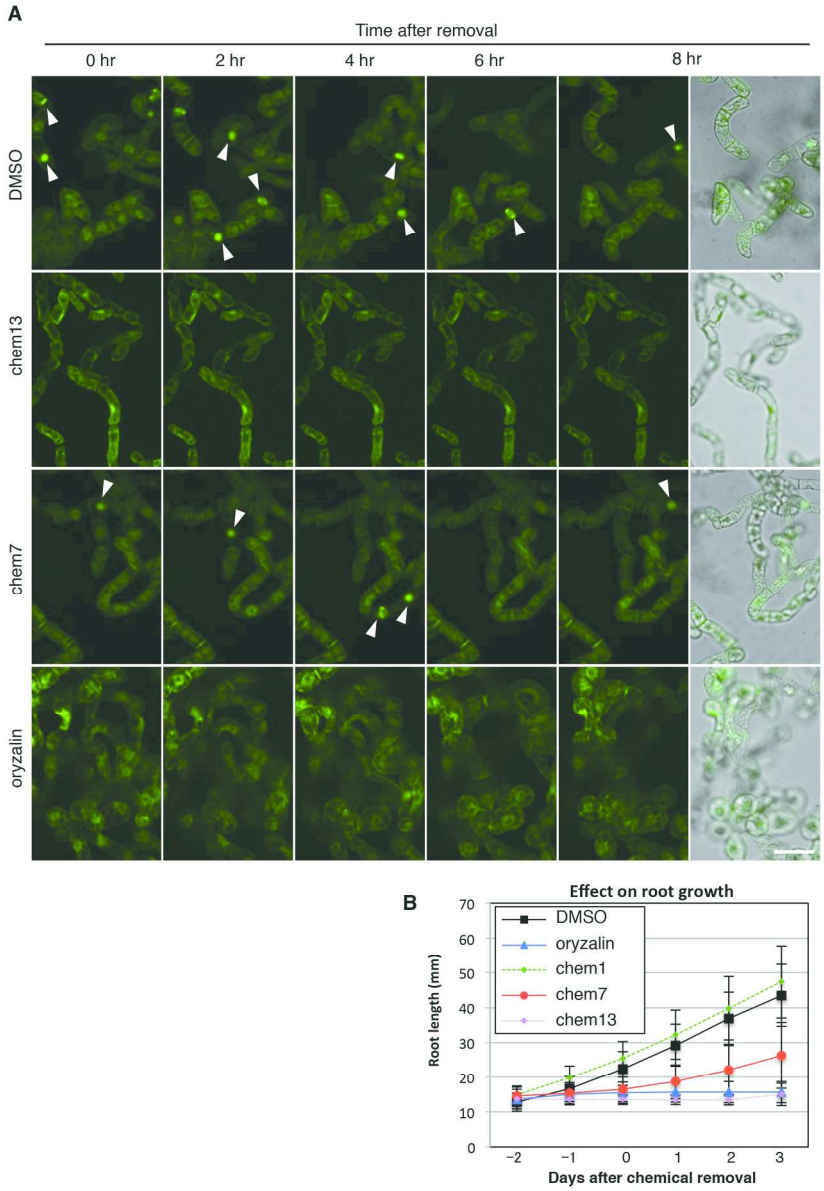

Fig. 6 Effect of (3-furyl)diphenylmethane is partially reversible.

172x247mm (300 x 300 DPI)

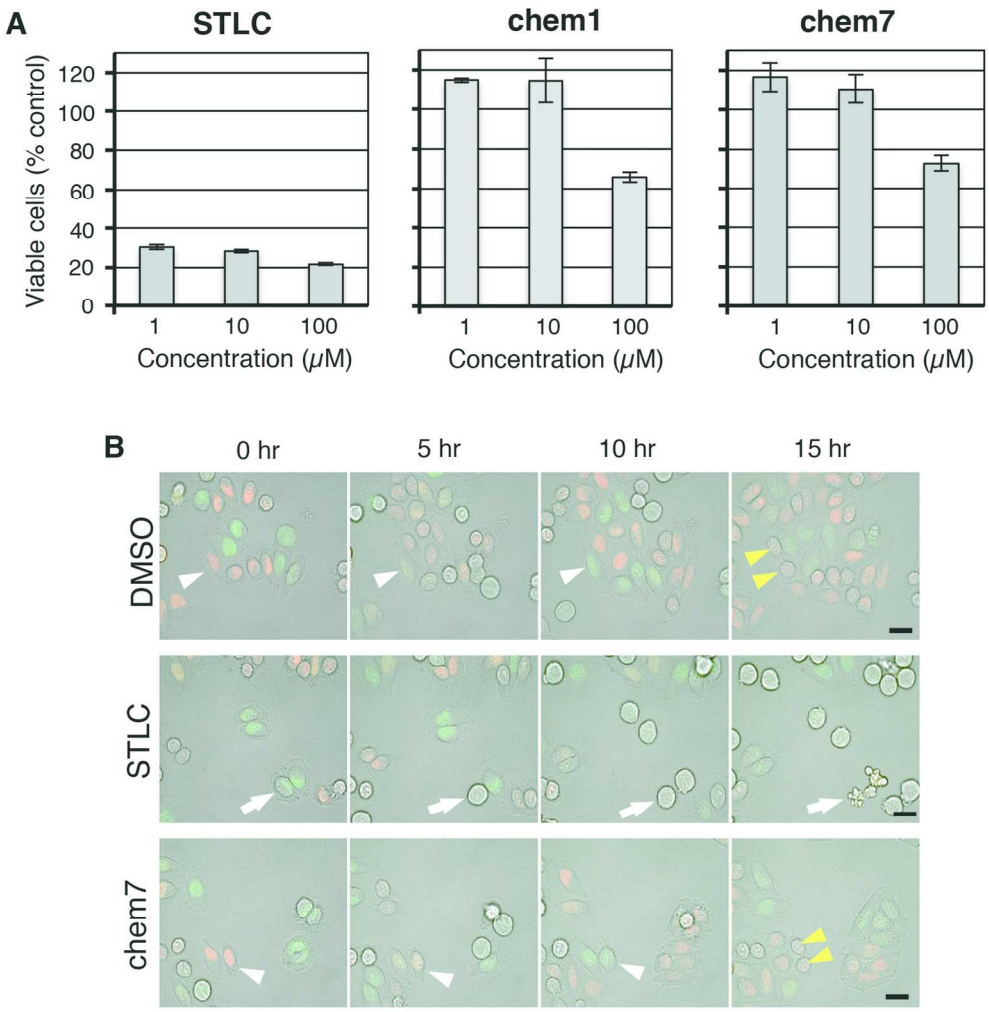

Fig. 7 (3-Furyl)diphenylmethane does not inhibit the growth of human cells.

140x143mm (300 x 300 DPI)

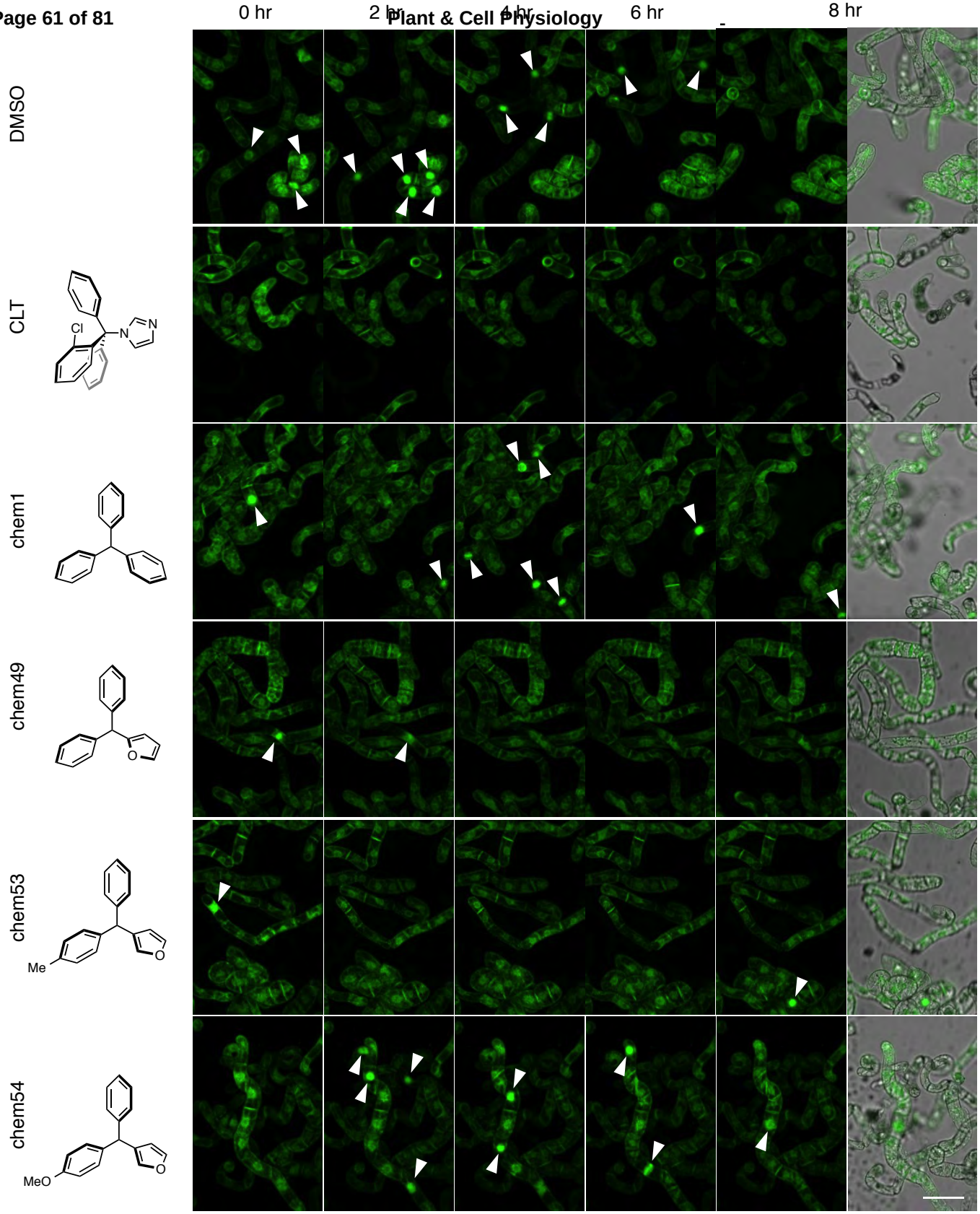

Supplementary Fig. S1 Effects of other triarylmethane derivatives.
Time-sequence observation of the cell division behavior of BY-GT16 in the presence of the indicated compounds. Arrowheads indicate dividing cells. The right panels are merged GFP and bright field images showing cell viability. Each compound was added at 100 μM in 0.1% DMSO. Scale bar, 40 μm.

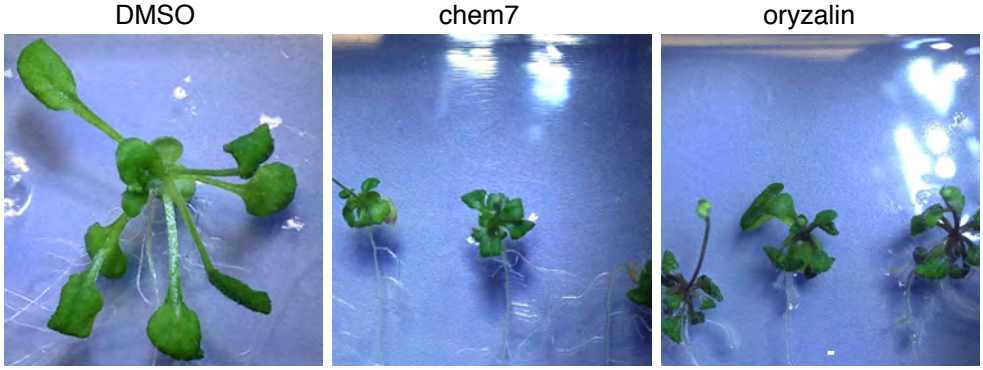

Supplementary Fig. S2 Effects of (3-Furyl)diphenylmethane on shoot growth.
Shoot structures of 21-day-old *Arabidopsis thaliana* plants (16 days after application of the indicated compounds). Oryzalin and chem7 were added at 1 and 100 μM, respectively, in 0.1% DMSO. Scale bar, 1 cm.

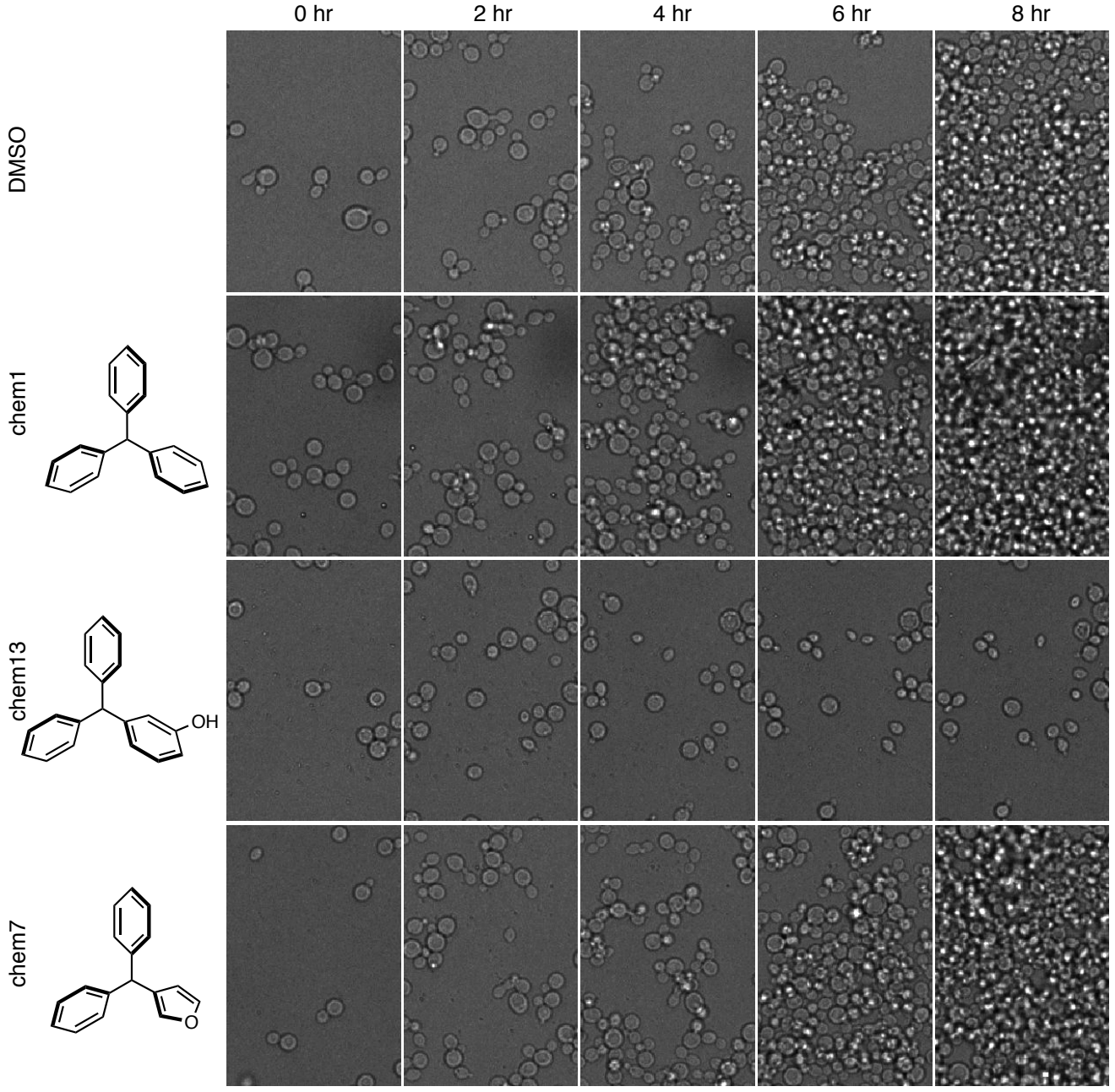

Supplementary Fig. S3 (3-Furyl)diphenylmethane does not inhibit the proliferation of yeast. Time-sequence observation of the proliferation of a budding yeast (*Saccharomyces cerevisiae*) in the presence of the indicated compounds. Each compound was added at 100 μM in 0.1% DMSO. Scale bar, 10 μm.